Gelation of Ionic Liquids with Silica Nanoparticles: The Role of Cation Structure and Interactions

Esteban Rucavado Leandro

Department of Applied Physics
Chalmers University of Technology
Göteborg, Sweden, 2011.

Gelation of ionic liquids with silica nanoparticles: The role of cation structure and interactions.

ESTEBAN RUCAVADO LEANDRO

Department of Applied Physics
Chalmers University of Technology
SE-412 96 Gothenburg
Sweden
Telephone : +46 (0) 31 772 1000

This thesis was done under the framework of "Erasmus Mundus Master in Nanoscience and Nanotechnology, EMM-Nano" within the trajectory of Katholieke Univesiteit Leuven, Belgium and Chalmers University of Technology, Sweden.

Abstract

This project investigates the gelation of ionic liquids using silica nanoparticles. The overall aim is to learn more about the ion-ion and ion-silica interactions in ionic liquid-silica dispersions and gels. Differences in the interactions between ionic liquid and silica are introduced by changing the structure of the cations. Four different ionic liquid based on imidazolium cation and [TFSI] anion have been used to gel silica nanoparticles. The structure of the cations is varied by changing the length and the end-group on the alkyl chain of the imidazolium ring, introducing e.g. the possibility of hydrogen bonding.

Each ionic liquid was found to have a different gel concentration, 3.8wt% for [C2MIM][TFSI], 4wt% for [EtOHMIM][TFSI], 3.5wt% for [C5MIM][TFIS], and 3.6wt% for [SMIM][TFSI]. At the gel concentration all samples were weak gels, showing a yield stress behaviour. Below 4wt% phase separation was observed for the [EtOHMIM][TFSI] silica dispersions.

The gelation of the dispersions does not have any dramatic influence on the properties of the ionic liquid. The glass transition temperature does not change and the conductivity decreases only slightly. Raman spectroscopy shows that there are no changes on the strong Raman band at 740 cm^{-1} (expantion-contraction of the entire [TFSI] anion) with silica concentration. From the results obtained, it is possible to conclude that in the gel, the silica matrix acts as a "container" for the ionic liquid: immobilizing the ionic liquid without making important changes to the properties.

Keywords: ionic liquid gel, silica, imidazolium, bis(trifluoromethylsolfonyl)imide, phase behavior, ionic conductivity, glass transition.

Acknowledgment

First of all I want to thank Aleksandar Matic for his supervision during the whole course of this thesis. Secondly I want to thank Jagath Pitawala, Jonas Nordström and Ezio Zanghellini for their guidance and assistance during this semester, this work would not be possible if not for their help. I also want to thank to the whole Condensed Matted Department Physics group for creating a great work environment.

I want to thank my mother, father and brother: for being my support during these years of absence. I have become the person I am thanks to them. Even though there were thousands of kilometers and two years between us, my love for them has no limits in distance nor time. I want to thank the rest of my family as well, specially to Silvia who was my role model, and to Valeria and Mariana, for whom I want to be role model.

I want to thank my family away from home, all those people who were present for me in these years when I really need them: Luis, Dries, Calle, Sofia, Chandra, Adrian, Kornelia, Andre, Aniruddha, Federico, and many others.

Also many people helped me in one way or another to fulfill this work, from Costa Rica and many other locations around the world. Thanks to: Gaby, Nella, Gera, Cojal, Bermu, Laura, Natis, Lucía, Manu, Lia, Ana, Dennis, Monte. A special thanks to my dear: “Chone-group” who I remember every time I did/say something wrong or inappropriate.

Finally I would like to thank the European Commission for creating and supporting a program such as Erasmus Mundus Master in Nanoscience and Nanotechnology, which allows young people from overseas to study and improve themselves.

Table of Content

I. Introduction

In Ionic Liquid Gels, a network of a dispersed phase is swollen with an ionic liquid (IL). The dispersed phase can be a polymer or colloidal particles. Even thought there are some reports on the applications of ionic liquid gels [1, 2], little is known about the basic interaction between the dispersed phase and the continuous phase in colloidal dispersions of this type and about the mechanisms controlling the gelation. These issues will be addressed and investigated in the present work.

Ionic liquids are also of interest from an applied point of view. Efforts have been made to develop new electrolytes, that are able to provide high ionic conductivity together with chemical, thermal, and mechanical stability. Solutions based on ionic liquids may satisfy the requirements needed for applications in batteries and fuel cells. In order to apply ionic liquids in a battery or a fuel cell [2-5], it is an advantage to have a solid electrolyte and to control the mechanical properties. This can be achieved with ionic liquid gels.

In the present work, silica nanoparticles were used to make gels with four different imidazolium based ionic liquids. The influence of silica nanoparticle concentration on physical properties such as ion conductivity, glass transition temperature, and molecular interactions in the ILs has been investigated. The used ionic liquids are based on the imidazolium cation, and the bis(triflourosulfonyl)imide anion. Each cation has a different side chain on the imidazolium ring, and the end group of this chain is also different. In addition to straight forward results about phase behavior, glass transition, ionic conductivity, gel concentration, and molecular interactions for the different ILs, the analysis performed on these suspensions and gels give an insight in how silica interacts with the ionic liquids, and how the cations and anions interact with each other.

This thesis is divided into six chapters. After the introduction, the second chapter describes basic concepts of ionic liquids and ionic liquid gels. It also summarizes the

research done previously on nano-silica ionic liquid gels. In the experimental chapter, the materials used, the sample preparation, and characterization techniques (Differential Scanning Calorimetry, Dielectric Spectroscopy and Raman Spectroscopy) are discussed. The results and discussion chapter is an extended description of the experimental results, their interpretation concerning gelation concentration, phase separation, glass transition behavior, ionic conductivity, molecular interactions, and particle size. The conclusions chapter summarizes the results obtain in this work. Finally, there is a chapter giving recommendations for further work.

II. Ionic Liquids and Ionic Liquid Gels

A. Structure and Properties of Ionic Liquids.

Ionic liquids are molten salts, i.e. liquids composed entirely of ions, with melting temperatures below 100°C [6]. There is a broad range of applications for ionic liquids. They may act as catalysts for chemical reactions, solvents for bioscience studies, or electrolytes for batteries and fuel cells [7]. Some of the properties that make ionic liquids interesting are: non-flammability, negligible vapor pressure, thermal stability, chemical stability, and high ionic conductivity [8, 9].

Table 1. Melting temperatures of some salts and common ionic liquids

Salt/IL	**Melting Temperature (°C)**
NaCl	803
KCl	772
[C3MIM]Cl^-	65
[C3MIM][PF_6]	10
[C3MIM][TFSI]	-22

Typically, an ionic liquid consists of a bulky asymmetric organic cation and a charge delocalized anion. The asymmetry and the charge delocalization results in weak electrostatic interactions, resulting in a low melting point. Table 1 presents some examples of melting temperatures of some common salts and ionic liquids, showing how the melting point is closely related to the size and shape of the anion and the cation [6]. If the anions and the cations are small, they are able to pack efficiently to form crystal structures with high melting temperatures (such as NaCl). As the size of the ions increases, the packing becomes less efficient, hence the melting temperature decreases, (such as 1-Butyl-3-methylimidazolium terafluoroborate).

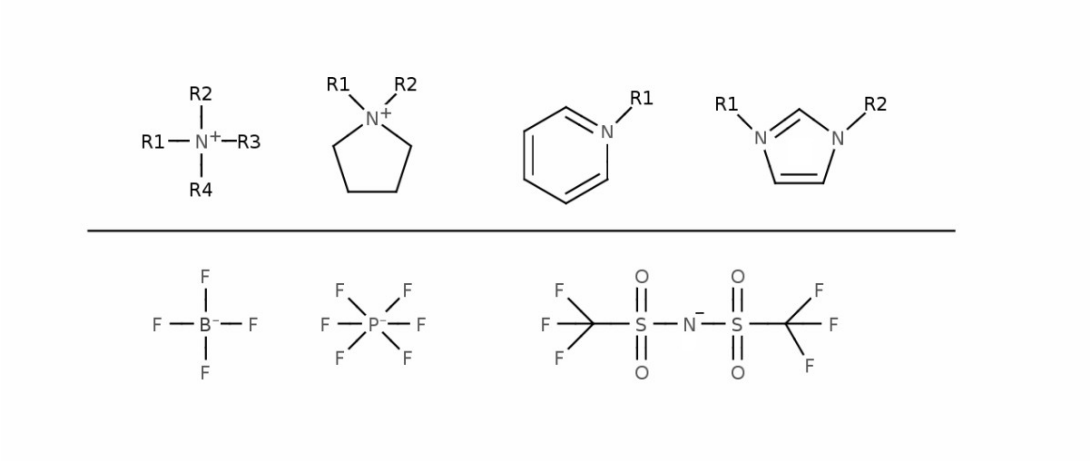

Figure 1. Some commercially available anions and cations. Top from left to right: tetraalkylammonium, N-alkyl-N-alkylpyrrolidinium, 1-alkylpyridinium, 1-alkyl-3-alkylimidazolium. Bottom: tetrafluoroborate, hexafluorophosphate, bis(trifluoromethanesulfonyl)imide .

Typical cations are made from nitrogen-containing organic aromatic rings with linear alkyl side chains. Ionic liquids with cations such as tetraalkylamonium, alkylpyrrolidinium, alkylimidazolium and alkylpyridinium are commercially available, see Figure 1. Most anions are polyatomic, inorganic, and have delocalized charge. Some commercially available anions are tetrafluoroborate, hexafluorophosphate and bis(trifluoromethylsulfonyl)imide, see Figure 1.

To facilitate further reading of this thesis, a common short-hand notation is used for ionic liquids. Imidazolium-based cations are denoted as [CnMIM], where n is the number of carbon atoms in the linear alkyl chain, for example, [C5MIM] is notation for 1-Pentyl-3-methylimidazolium. Anions such as tetrafluoroborate, hexafluorophosphate and bis(trifluoromethylsulfonyl)imide are denoted as [BF_4], [PF_6], and [TFSI] respectively.

The possibility to independently change the molecular structure of anions and cations allows the design of millions of different ionic liquids with different properties. With small changes in the structure of the ions, it is possible to tune the physicochemical properties to make an useful material for a specific application. For this reason ionic liquids are considered as “designer solvents” [6]. For example, a small change in the alkyl chain in alkyl-methylimidazolium ionic liquids can considerably change the viscosity, the glass transition temperature, and the ionic conductivity. As an example of this, the glass transition temperature of 1-(4-sulfobutyl)-3-methylimidazolium bis(trifluoromethasulfonyl) imide is -56°C; while for [C5MIM][TFSI] is -85°C. The only difference between these ionic liquids is a SO_3H group at the end of the alkyl chain for the 1-(4-sulfobutyl)-3-methylimidazolium bis(trifluoromethasulfonyl)imide. The structures of the cations are shown in figure 4, Chapter 3.

Commonly ionic liquids are divided into two categories, protic and aprotic [6]. Synthesis of aprotic ionic liquids is a two step process. First a tertiary amine is alkylated by adding an alkyl chloride, then the chloride ions are exchanged with the required anion to form a salt with low melting temperature. This is called the quaternization method. Since this synthesis consist of two steps is easy to form byproducts in the ionic liquid that will lower the purity of the final product. In the synthesis of protic ionic liquids, the cations are obtained from the transfer of a proton from a Brønsted acid to a Brønsted base in a neutralization process. Since it is a one step process, there is less need for purification. Figure 2 shows schematically the two different synthesis processes.

For the scope of this work, it is important to differentiate between the cation structures of the ionic liquids, due to their influence on the physical properties of ionic liquid suspensions and gels. Naturally, it is expected that the different ionic liquids will have different interactions. The presence of an extra OH group on the cation of the protic ionic liquid, can create interactions via hydrogen bonding. Thus different anion-cation interactions as well as interactions with the silica

nanoparticles are expected.

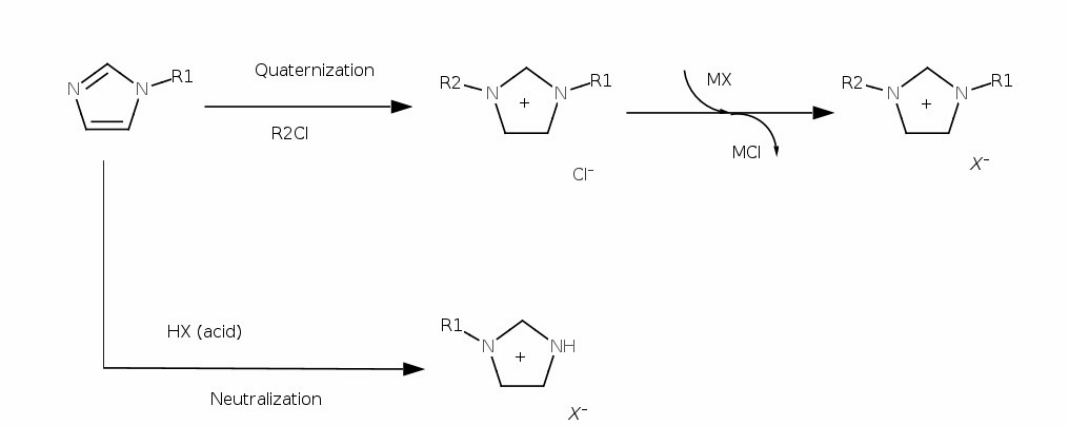

Figure 2. Synthesis of protic and aprotic imidazolium based ionic liquids. The product of the quaternization process is an aprotic ionic liquid while the product of the neutralization process is a protic ionic liquid.

B. Ionic Liquid Gels

The present work investigates properties of ionic liquid dispersions and gels. The particles in a colloidal dispersion are small (1nm - 10 μm), thus they have a high surface area [10]. At high enough concentrations the particles will interact with each other and can form a gel. Even though there are several definitions of what a gel is [11] for the purpose of this work we shall consider a gel as a colloidal dispersion which exhibits the mechanical characteristics of a solid, where both the dispersed component and the dispersion medium extend continuously throughout the whole system [12]. To determine if a sample is a gel or not, a simple experiment is done in which the tube containing the sample is turned upside-down. If the sample does not flow it is considered to be a gel. [13]. A more rigorous determination is a investigation of the elastic modulus (G') which should exhibit a plateau extending to times at least of the order of seconds, and the viscous modulus (G") which should be considerably smaller than the elastic modulus in the plateau region [11].

Previously, research has been done with ionic liquids and silica nano-particles in the gel state [13-18]. The group of Watanabe has contributed the most, by studying the

colloidal stability, ionic transport, rheological properties, surface chemistry, and microstructure of colloids in ionic liquids [13-19]. Rheology studies showed that, for [C2MIM][TFSI] containing 5wt% of hydrophilic silica nanoparticles, G' is frequency-independent and higher than G" for one order of magnitude, indicating that the colloidal suspension behaves as a solid-like material, i.e. as a gel [13]. In contrast, [C4MIM][BF4] suspensions with 15wt% hydrophilic silica showed frequency-dependence on both G' and G", with the viscous modulus higher than the elastic modulus, indicating that even at this high concentrations, the dispersion behaves as a liquid-like material [13]. The shear rate dependence of viscosity was measured for [C2MIM][TFSI] and [C4MIM][BF4] hydrophilic silica dispersions, showing shear thinning for [C2MIM][TFSI] with a 5wt% silica concentration. For [C4MIM][BF4] 5wt%, 8wt%, 10wt%, and 15wt% [13] the viscosity is constant at low shear rates, but in increases drastically at high shear rates. This shear thickening behavior is enhanced by the silica concentration i.e. with a higher concentration the steeper is the increase. Using hydrophobic silica, dynamic oscillatory shear measurements showed that in both types of IL, G' was higher than G", indicating a soft-solid behavior even for concentrations as low as 5wt%. The shear rate dependence of viscosity showed that, when using hydrophobic nanoparticles, the gels exhibit shear thinning, also for [C4MIM][BF4] [13]. These results suggest that both anions and cations may interact with silica, for instance with hydrogen bonding and electrostatic interactions. This may create steric hindrance and/or solvation forces which stabilize the colloidal particles in the ILs.

Work has also been done on the physical properties of soft glassy colloidal arrays consisting of polymer grafted silica nanoparticles and ionic liquids [17]. It has been demonstrated that at low concentration, the polymer grafted particles are well suspended in the ionic liquid without aggregation or sedimentation, and they show a liquid-like behavior. However when the concentration is increased up to 14.2 wt%, the suspension becomes solid. This type of suspensions (or gels) also exhibit different colors that depend on the particle concentration: red, green and blue for concentrations of 14.2wt%, 25.0wt%, 33.3wt% respectively [17]. For [C2MIM]

[TFSI] and polymer grafted silica nanoparticles (using side chains of poly(benzyl methacrylate) and poly(methyl methacrylate) attached to the surface of the particle), it was found that depending on the structure of the grafted polymer and the nanoparticle concentration, the colloidal array might phase separate at certain temperature [16].

Theoretical estimations of the colloidal interactions between silica particles in ionic liquids have been performed using the Derjaguin-Landau-Verwey-Overbeek (DLVO) theory [15]. With the DLVO theory and Dynamic Light Scattering experiments, it was demonstrated that bare silica particles cannot be stabilized and form aggregates in different imidazolium bases ionic liquids. The stability of bare silica particles was compared with the colloidal behavior of polymer grafted nanoparticles, which showed good colloidal stability for [C3MIM][PF_6] and for imidazolium [TFSI] ionic liquids [15]. Steric forces may cause the stabilization of PMMA grafted silica nanoparticles [15].

The group of Liu has studied the immobilization of imidazolium based ionic liquids on silica nanoparticles using DSC, X-ray diffraction, and Raman spectroscopy [14]. Studied cations are [C2MIM], [C3MIM], and [BenzylMIM]. They found that the melting point of the immobilized ionic liquids decreases considerably compared with the pure ionic liquid. They conclude that this is caused by hydrogen bonding networks between the cations and the nano-Silica.

The silica particles can interact by Van der Waals forces, electrostatic interactions, and hydrogen bonding. The energy of the H-bond is dependent on the O-H-O angle and can vary between 20-25 kJ/mol [19], with a maximum energy when the angle is zero. In A200 nanoparticle dispersions, the creation and breaking of H-bonds might be able to explain the rheological properties in a solvent such as ionic liquids [14]. Figure 3 shows how surface silanol groups between two primary silica nanoparticles can interact.

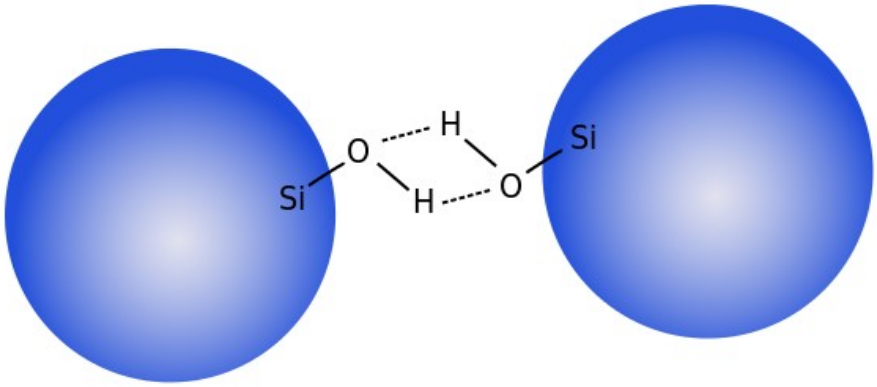

Figure 3. Hydrogen bond between two idealized A200 primary nanoparticles. (figure is not in scale)

In protic and aprotic ionic liquids, hydrogen bonding has an important role by stabilizing the ionic liquids suspensions and gels. It has been suggested that in aprotic ionic liquids, hydrogen bond networks are formed between cations (such as [C2MIM], [C3MIM], [C6MIM]) and the surface silanol groups of the Silica nanoparticle [14] . On the other hand, for protic ionic liquids, a different interaction is expected since the presence on OH groups on the cation creates hydrogen bonds between the A200 nanoparticles and the cation but also a stronger anion-cation interaction.

1. Colloidal Interactions

One factor affecting the stability of a colloidal suspension is gravity. If the dispersed particles are denser than the liquid they will tend to sediment. On the other hand, if the particles are less dense than the liquid they will tend to rise to the surface. Such behavior is known as creaming [10]. Thermal motion of the particles (Brownian motion) counteracts gravity, by randomizing the displacement of the particles in the medium, hence preventing creaming or sedimentation of the colloidal dispersion

In addition to gravity and Brownian motion, there are attractive, and repulsive, long-range and short-range forces in colloidal dispersions that will determine their

behavior. Particles with a surface charge will result in repulsive forces. However in an electrolyte, a solvation layer will form around the particles. As a result the surface charge of the particles will be screened. The distance that characterizes this electrostatic screening in a colloidal dispersion is the Debye screening length, κ^{-1}:

$$\kappa^{-1} = \left(\frac{\varepsilon_r \varepsilon_0 k_B T}{2e^2 n_0 z^2} \right)^{1/2} \quad (1)$$

where z is the charge of the ions in the solution, n_0 is the ion concentration in the solvent, ε_r the dielectric constant of the solvent, k_B is the Boltzmann constant, and ε_0 is the dielectric permittivity in vacuum. The screening of the surface charge will destabilize the dispersion, leading to aggregation of the particles. Besides the screening, there are more ways to control the stability in a colloidal dispersion, such as changing the pH in the solution, grafting the particles with polymers, or even adding polymer coils to the solvent [18].

It has been reported that cations and anions in ionic liquids may interact with silica nanoparticles through hydrogen bonding [13,14]. Hydrogen bonding is a form of association between an electronegative atom and a hydrogen atom attached to a second, relatively electronegative atom. The electronegative atoms are usually nitrogen, oxygen, or fluorine. The associated energy in hydrogen bonds are usually 20–25 kJ mol^{-1} [19], which is one order of magnitude more than the room temperature thermal energy (2.4 kJ mol^{-1}). In the context of this work, hydrogen bonds are important because it is believed that the hydroxyl groups on the surface of the silica particles can form hydrogen bonds with the ionic liquid, forming an ordered solvation layer around the particles which influences surface interactions and thus the phase behavior of the ionic liquid silica dispersion [14] [20]. In literature we find [13,14] that some ionic liquids that might form hydrogen bond with surface silanol groups are [C2MIM][PF6], [C3MIM][PF6], [EtOHMIM][TFSI] and [BenzylMIM][BF4].

III. Experimental

This chapter describes the materials and experimental techniques that are used to characterize the ionic liquid gels and suspensions. Differential Scanning Calorimetry (DSC) was used to determine the glass transition temperature (T_g) of pure and gelled ionic liquids. Dielectric Spectroscopy was used to investigate the ionic conductivity. Finally, ion-ion and ion-silica interactions of the materials were studied using Raman spectroscopy.

A. Materials

1. Ionic Liquids

For this work four ionic liquids were used, with different cations but the same anion. The cations are: 1-(4-sulfobutyl)-3-methylimidazolium, 1–Pentyl–3-methylimidazolium, 1–ethanol–3-methylimidazolium, and 1-ethyl-3-methylimidazolium. The common anion is bis(trifluoromethasulfonyl)imide. To facilitate reading, the following abbreviations, will be used for cations and anions: [SMIM] for 1–(4-sulfobutyl)–3-methylimidazolium, [C5MIM] for 1–Pentyl–3-methylimidazolium, [EtOHMIM] for 1– ethanol–3-methylimidazolium, [C2MIM] for 1-ethyl-3-methylimidazolium and [TFSI] for bis(trifluoromethasulfonyl)imide. Figure 4 summarizes the molecular structures of the cations and the anion. All the ionic liquids were purchased from Solvionic Corporation and they were stored in the glove-box.

These ionic liquids were chosen in order to compare the influence of the cation structure, and in particular hydrogen bonding, on the ionic liquid/silica dispersion and gels. Each cation contains one imidazolium ring and an alkyl chain. The [C5MIM][TFSI] and [SMIM][TFSI] have a similar molecular structure, the only difference is a sulfonic acid group at the end of the alkyl chain for [SMIM].

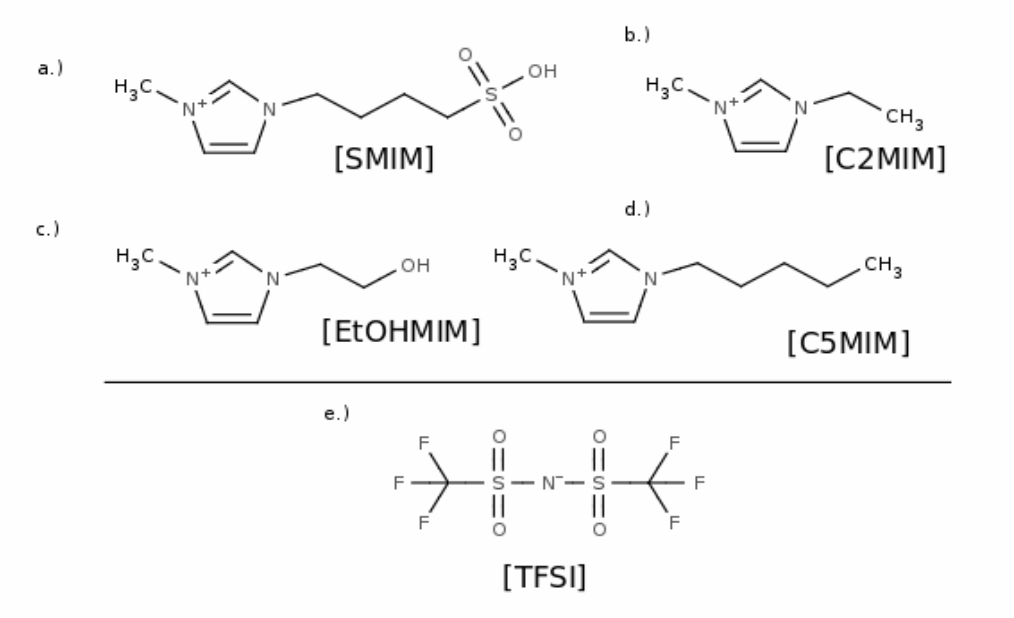

Figure 4. Molecular structure of the cations and the anion used in this work.

In a similar way, the only difference between [C2MIM][TFSI] and [EtOHMIM] [TFSI] cations is a OH group at the end of the alkyl chain in [EtOHMIM][TFSI]. Table 2 shows some properties reported in literature of the ionic liquids.

Table 2. Physical properties of the four ionic liquids. For some of the ionic liquids, data is not available in literature.

Property	**[C5MIM] [TFSI]**	**[SMIM] [TFSI]**	**[C2MIM] [TFSI]**	**[EtOHMIM] [TFSI]**
Molecular Weight	433.39	499.43	391.32	407.32
Density (g/cm^3) @ RT	1.403 [21]	-	1.52 [22]	1.57 [23]
T_g (K)	188.15 [21]	217.1	181.15 [22]	194 [23]
T_m (K)	264.15 [21]	-	256.15 [22]	-
Viscosity (cp) @ RT	-	-	34 [24]	85.5 [13]

2. A200 Silica Nanoparticles.

The A200 nanoparticles were obtained from Evonic Industries. A200 nanoparticles are large-scale industrial fabricated by continuous flame hydrolysis of silicon tetrachloride ($SiCl_4$). In the flame hydrolysis, $SiCl_4$ is converted to the gas phase and reacts spontaneously in an oxyhydrogen flame with the intermediately-formed water to produce the silicon dioxide [25]. By changing the exposure time, concentration of reactants and flame temperature it is possible to tune the particle size, size distribution, and surface area.

During the flame exposure, small primary particles with sizes between 5 and 40 nm are formed. These primary particles bond covalently in a fractal form to create the final product of this process, a fractal aggregate of primary particles with typical diameters 200-300 nm and surface areas between 50 - 400 m^2/g [25]. Figure 5 illustrates the fractal arrangement of the primary nanoparticles.

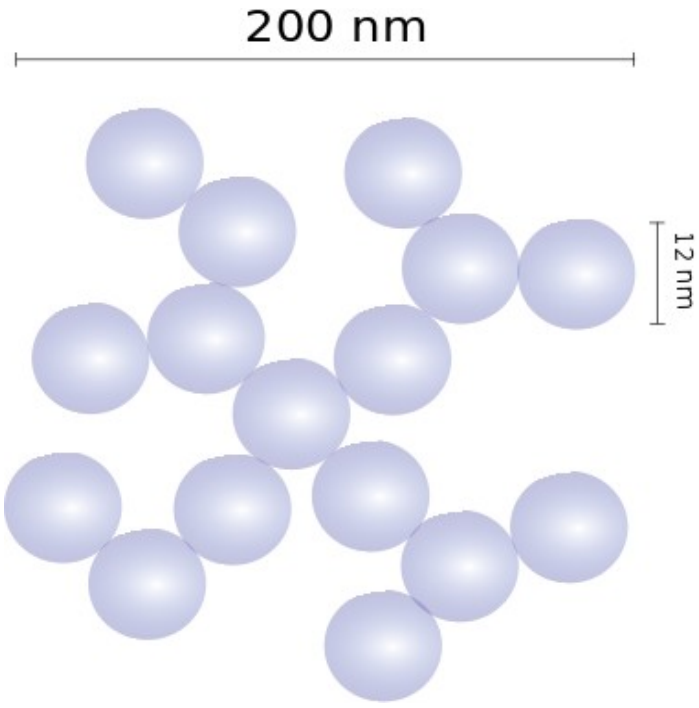

Figure 5. Fractal arrangement of the covalently bonded primary particles in A200.

An important characteristic of fumed silica is the high surface area which dependents on the average size of the primary nanoparticles. The surface has two functional groups: silanol and siloxane, see Figure 6. Silanol groups have a hydrophilic character while siloxane groups are hydrophobic. Without after-treatment of A200, there will be more silanol groups at the surface and the particles are hydrophilic.

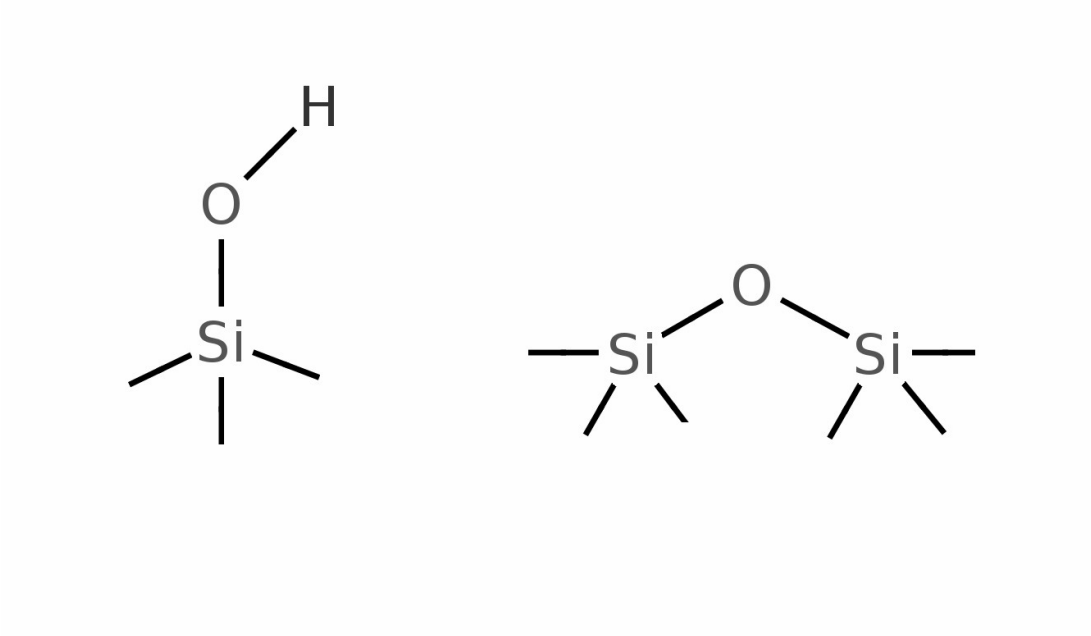

Figure 6. Functional groups of the silica nanoparticles at the surface. Silanol (left) presents a hydrophilic behavior while siloxane (right) gives a hydrophobic character.

B. Sample Preparation

Before the A200 nanoparticles were used, they were dried for approximately 24 hours at 150°C in vacuum. The mixing of the ionic liquids and the nanoparticles was performed in an argon-filled glove-box.

The concentration of A200 in the samples are reported in weight percent (wt%) of silica to the weight of the ionic liquid. The silica nanoparticles and the ionic liquids were mixed and stored in previously cleaned vials. Just after preparation of the

samples, the vials were para-filmed to avoid oxygen and water contamination. All the samples were stored outside the glove-box.

An ultrasonic after-treatment for 2 hours was performed on all samples. This was done in order to ensure an homogeneous dispersion of the nanoparticles in the ionic liquid. The maximum power of the ultrasonic bath is 950W.

C. Differential Scanning Calorimetry

Differential scanning calorimetry (DSC) is one of the most used thermal analysis techniques. Essentially, the main idea of this technique is to obtain information of thermal changes in a sample. The heat flow is determined when heating (or cooling) the sample and a reference at a specific heating (or cooling) rate [26]. DSC can be used to obtain a wide range of information and on very different types of materials. For instance, DSC can be used to study polymers, glasses, ceramics, liquid crystals, biological materials, metals, alloys, minerals, pharmaceutical products, etc. For the purpose of this thesis, DSC measurements will be focused on the glass transition temperature (T_g). The next sub-chapter will shortly explain the glass transition and why it is important for this work.

The DSC instrument determines heat flow, derived from the temperature difference between the sample and a reference. During the measurements, the sample is placed in a crucible and the reference is either an inert material or an empty crucible. Two separate temperature sensors measure the temperature difference between the sample and the reference. This difference is converted into differential power using an algorithm in the software of the DSC instrument. The result of this is a thermal analysis curve in which the instrument signal is plotted against temperature. As an example of a DSC curve, Figure 7 shows the glass transition, the crystallization, and the melting of [C2MIM][TFSI]. The glass transition is observed as a change in the base line, crystallization is observed as two exothermic peaks whereas melting as two endothermic peaks. All DSC measurements in this thesis were performed using

a Q1000 TA instrument .

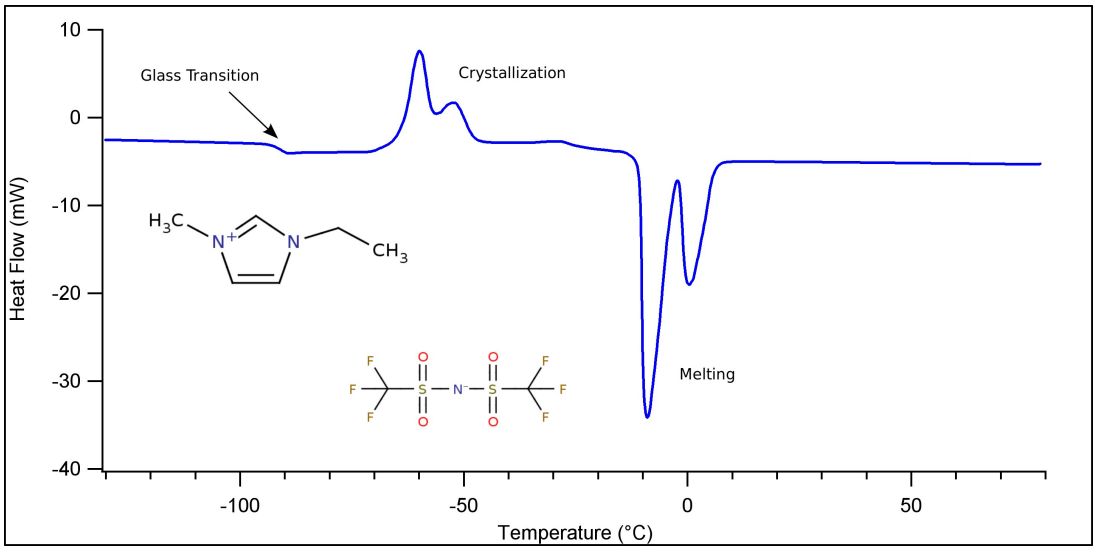

Figure 7. Example of a DSC curve from pure [C2MIM][TFSI]. The curve shows the glass transition, the crystallization, and the melting of the material.

1. The Glass Transition

Under some circumstances, it is possible to cool a liquid below the freezing point without crystallization. This is possible if the cooling rate is fast enough to avoid crystallization, or if the nucleation rate is very low [10]. At some temperature below freezing, there is a sudden change in the thermal expansivity or heat capacity of a liquid, this temperature is known as glass the temperature (T_g). The glass transition may be confused with a second order phase transition, but T_g is not a real thermodynamic phase transition since it depends on the heating (or cooling) rate. [10]

Experimentally, the glass transition is observed as a discrete change of the baseline in a DSC measurement [27]. In Figure 8 the glass transition of [EtOHMIM][TFSI] is shown. The value of T_g is -75.4°C for this ionic liquid. The glass transition is defined as the mid-point of the transition, where the slope is steepest.

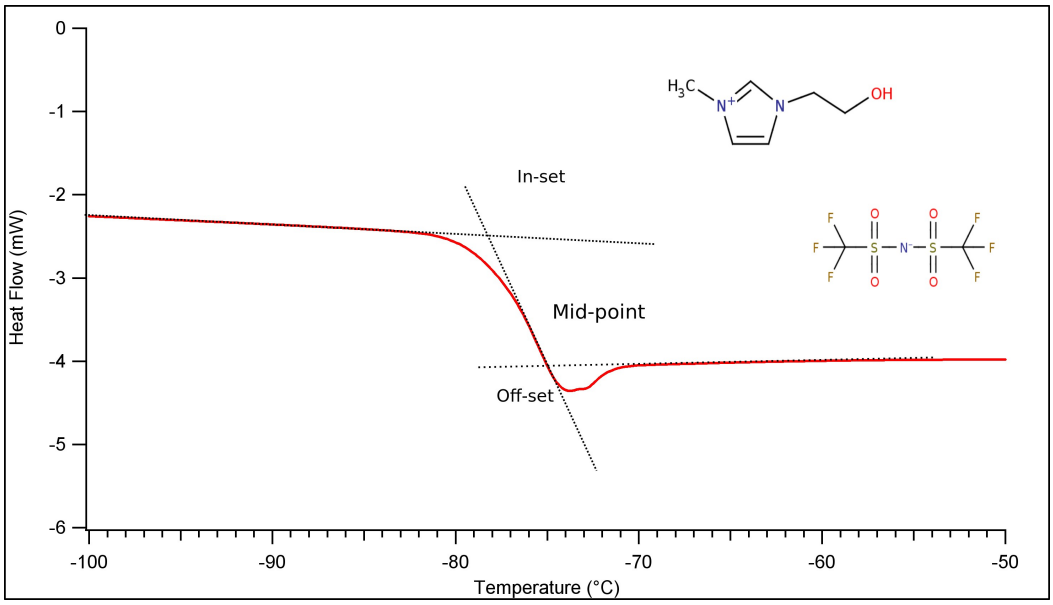

Figure 8. Determination of the glass transition temperature for [EtOHMIM][TFSI] pure ionic liquid, from the DSC experiment.

D. Dielectric Spectroscopy.

Dielectric spectroscopy measures the response of the dielectric permittivity of a material to an external oscillating electric field. When a field, $\mathbf{E}(\omega) = \mathbf{E}_0\exp(-i\omega t)$, is applied to a material, it will induce a dipole moment. This dipole moment is characterized by the electric polarization vector, **P**

$$P(\omega)=(\varepsilon_r-1)\varepsilon_0 E(\omega) \tag{2}$$

where ε_0 is the dielectric permittivity in vacuum ($8.85*10^{-12}$ As/Vm) and ε_r is the relative permittivity of the material. This polarization describes the dielectric displacement which originates from the response of the material to the field $\mathbf{E}(\omega)$. Considering small electric fields, the dielectric displacement **D** can be expressed as [28]

$$D=\epsilon^*\epsilon_o E \tag{3}$$

where ε^* is the dielectric function or dielectric permittivity. The dielectric function

is complex and frequency dependent.

$$\epsilon^*(\omega)=\epsilon'(\omega)-i\epsilon''(\omega) \tag{4}$$

By properly analyzing the dielectric function, it is possible to study effects such as orientation of the dipoles, polarization effects, and ionic conductivity of a material [30]. The conductivity is a result of an energy loss, hence is related to the imaginary part of the dielectric function [28].

$$\sigma'(\omega)=\omega\varepsilon_0\varepsilon''(\omega) \tag{5}$$

When a material is under the influence of a field, the drift of the mobile carriers (such as electrons or ions) cause conductive contributions to the dielectric response. This response is characterized by a field displacement of the form $\mathbf{D} = \mathbf{D_0}\exp[i(\omega t-\delta(\omega))]$ where $\delta(\omega)$ is the phase shift and $\mathbf{D_0}$ is the amplitude of the displacement [28]. Considering this, it is possible to describe the permittivity as

$$\epsilon^*=\frac{D_0}{\epsilon_0 E_0}\exp[-i\,\delta(\omega)] \tag{6}$$

where E_0 is the magnitude of the applied electric field.

Typically for dielectric spectroscopy, the current is measured as a function of the applied voltage. The complex impedance is the ratio

$$Z^*(\omega)=\frac{U^*(\omega)}{I^*(\omega)} \tag{7}$$

Using the previous results, the complex dielectric function can be calculated as

$$\epsilon^*=\frac{-i}{\omega C_0 Z^*(\omega)} \tag{8}$$

Where, C_0 is the capacity of the empty cell. Using equation [7] and equation [8], the conductivity can be calculated.

The experiments were performed by placing the sample in a coin-shaped container, with electrodes at the top and the bottom of the coin. This cell has dimensions of 1.1 mm thickness and 13 mm diameter. The real part of the conductivity is plotted as a function of the frequency for different temperatures. Measurements were performed between 50°C and -100°C, at every 10°C (stabilization time of 900 s at each temperature). The frequencies range was from 10^7 to 10^{-2} Hz. As an example, Figure 9 shows the real part of the conductivity for pure [SMIM][TFSI].

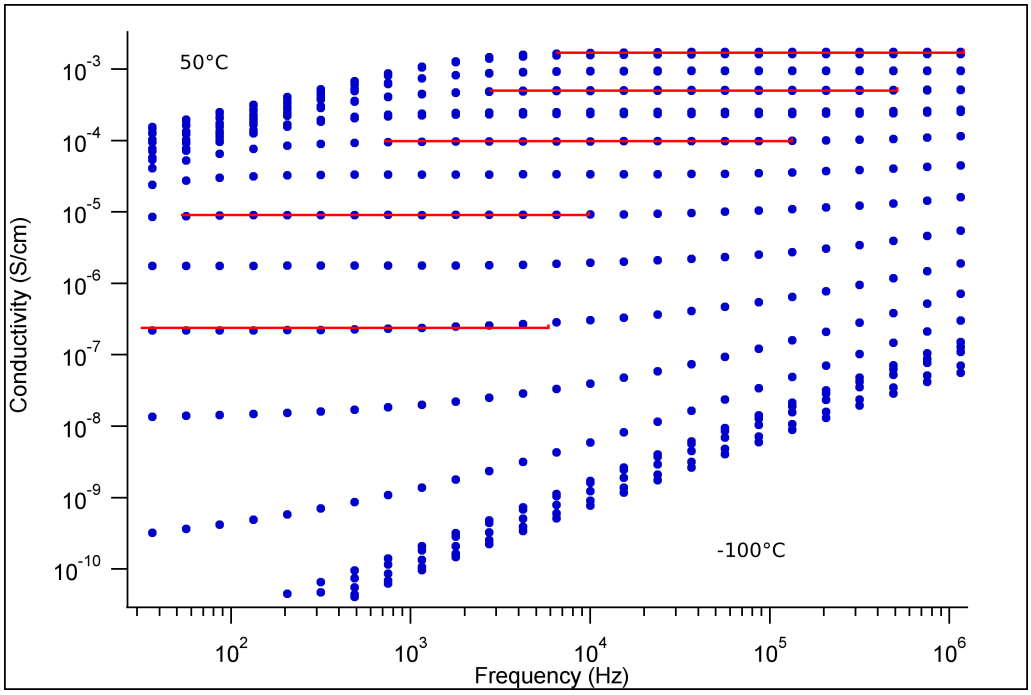

Figure 9. The real part of the complex conductivity (σ'). This measurement is as function of frequency and temperature. For the pure ionic liquid [SMIM][TFSI]. The DC-conductivity plateau is indicated by the red lines.

The DC-conductivity is obtained from the conductivity plot by using the conductivity value where there is a plateau over a range of frequencies. The DC-conductivity determined from the data in figure 9 is shown in figure 10. As it is expected for this type of systems, the conductivity increases with increasing temperature.

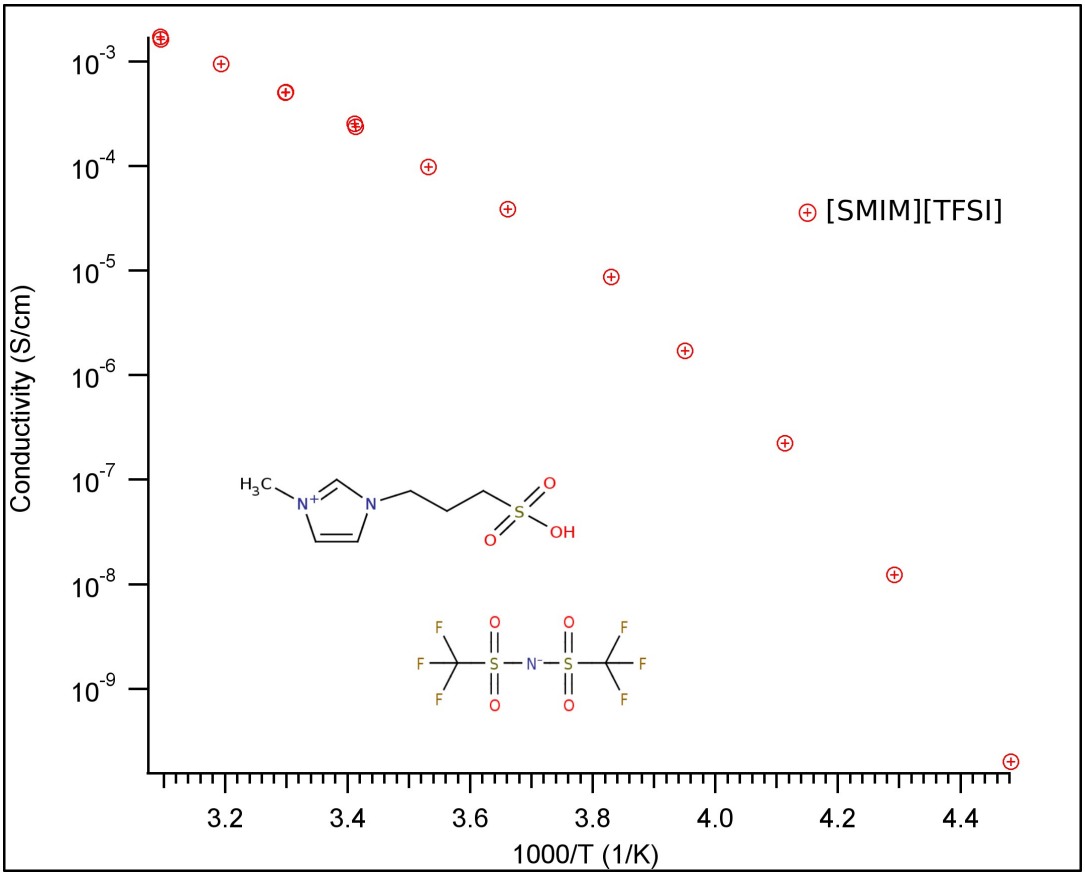

Figure 10. DC-conductivity plot for [SMIM][TFSI]. Each data point is extracted from a plateau of Figure 9.

E. Raman Spectroscopy.

Raman spectroscopy is used to provide information on chemical structures, to identify substances from the characteristic spectral patterns and to determine quantitatively or semi-quantitatively the amount of a substance in a sample. It can also be used to determine chemical and physical interactions in a material. Solid, liquid, or vapor samples can be examined using Raman spectroscopy. Modern Raman instrumentation has simplified the experiments. These advances, together with the ability of Raman spectroscopy to examine aqueous solutions and samples inside glass containers, makes Raman spectroscopy an ideal characterization technique for this work.

In Raman spectroscopy, a single frequency is used to irradiate a sample and the radiation scattered from the material, is detected. Unlike infrared absorption, Raman scattering does not require the energy matching of the incident radiation with the energy difference between ground and excited states [29]. During Raman scattering, the light interacts with the molecule, polarizes the cloud of electrons around the nuclei and forms an unstable state, "virtual state", from which, the photon is quickly re-radiated. If only electron polarization occurs, the photons will be scattered with a very small energy shift, since the electrons are light compared with nuclei. This process in known as Rayleigh Scattering [29].

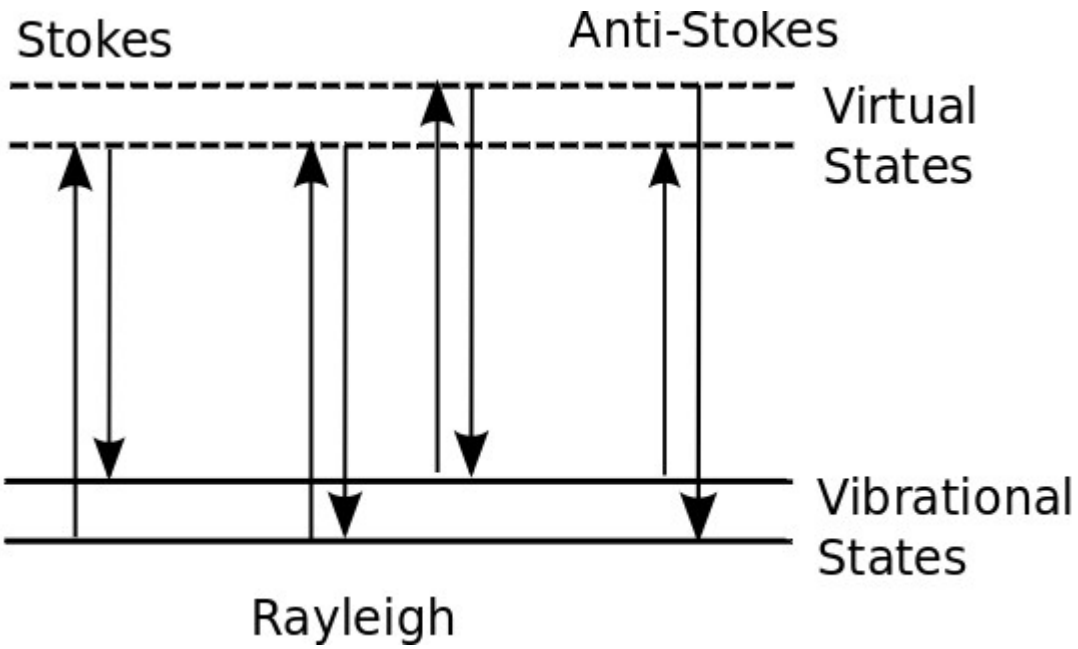

Figure 11. Rayleigh and Raman scattering processes. The virtual state is created when the light interacts with the electrons and causes polarization

However, if nuclear motion is induced, energy will be transferred from the incoming photon to the molecule or from the molecule to the scattered photon. This is an inelastic process since the energy of the scattered photon is different from that of the incident photon. This process is known as Raman scattering.

Figure 11 shows the basic processes that can occur. The energy of the virtual states

is determined by the frequency of the incoming light [29]. The Rayleigh process is more intense since a higher amount of photons scatter this way.

Stokes scattering occurs if the molecule has a higher vibrational state after the scattering process [29]. However, some molecules may be in an excited state, due to thermal energy, and the incoming light de-exites the molecule to the ground state, from this mechanism, the outgoing light generates anti-Stokes scattering. During this process, there is energy transfer to the scattered photon. At room temperature, molecules are expected to be in a lower vibrational state, so Stokes scattering will be more likely to occur than anti-Stokes.

The movement of molecules can be described with the degrees of freedom. Three degrees of freedom describe the translation in space of the molecule (the Cartesian coordinates in three dimensions), and three describe rotational movements (except for linear molecules, that only need 2). If there are N atoms in a molecule, the number of vibrational degrees of freedom, and therefore the number of vibrations possible, is 3N-6, except for linear ones where it is 3N-5 [29].

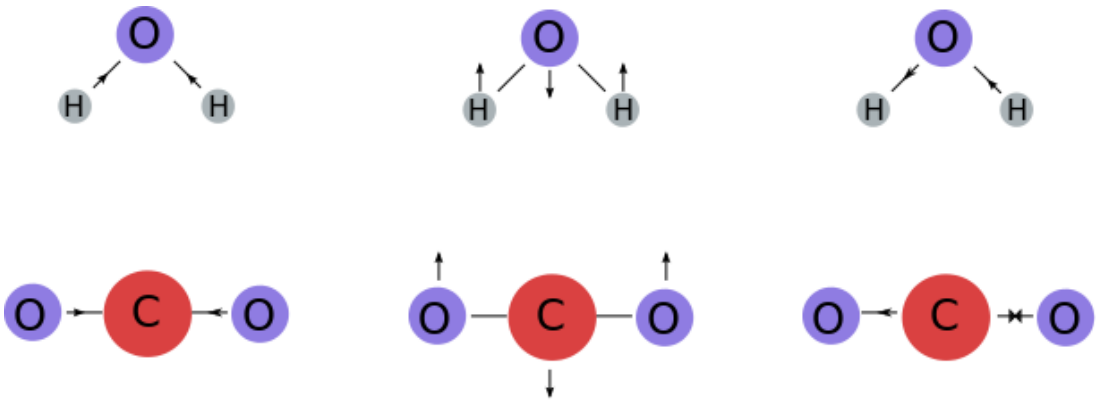

Figure 12. Spring and ball model for three vibration modes for water and carbon dioxide. From left to right, symmetrical stretch, bending, and asymmetric stretch.

There are two types of vibration modes, the stretching mode and bending mode. Figure 12 shows stretching modes (those where the bond length increases and decreases within the bond axis), the symmetrical and asymmetric stretch. In the

bending vibration, there is a change in the angle between the bonds of the molecule [29]. Bending mode can be divided in 4 categories: rocking, scissoring, wagging and twisting modes.

In the present study, Raman spectra were recorded using a Bruker IFS66 Fourier Transform Spectrometer using the 1064 nm line of Nd:YAG laser. A germanium detector was used to detect the scattered light. The power of the laser was 400 mW and the resolution was set to 2 cm^{-1}. The Raman measurements were performed at room temperature

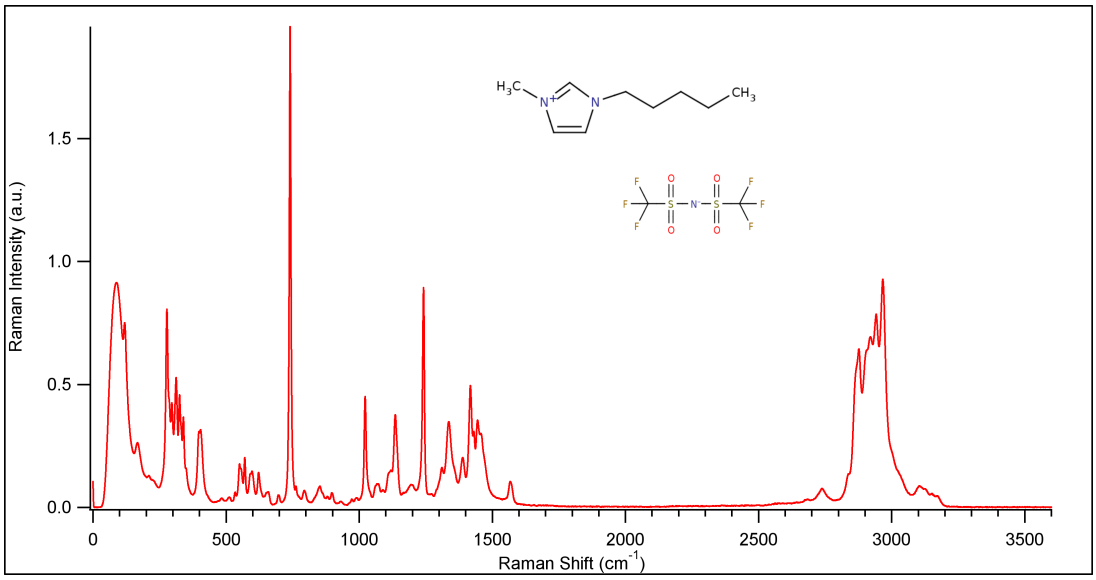

Figure 13. Stokes *spectrum for [C5MIM][TFSI]. The inset shows the structure of the anion and the cation.*

With Raman analysis it is possible to investigate the ionic interactions and conformations within the ionic liquid. In this work there is a special interest in the 740 cm^{-1} band, which corresponds to the expansion and contraction mode of the hole [TFSI] anion [30].This band may be shifted because of ionic interactions or by a change in the conformation state of [TFSI]. The two conformations of this particular anion will be discussed in detail in chapter IV. Figure 14 shows a zoom-in of the 740 cm^{-1} band for the pure ionic liquid [C5MIM][TFSI].

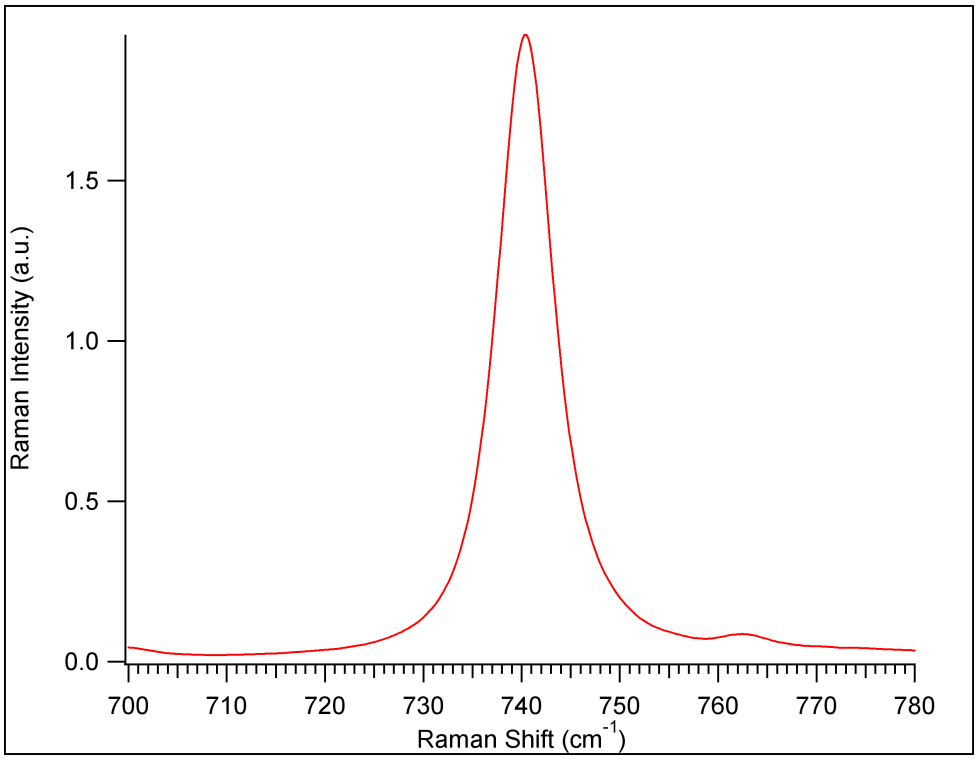

Figure 14. Zoom in of the 740 cm⁻¹ band for [C5MIM][TFSI]. This band corresponds to the expansion and contraction of the whole TFSI anion [30].

IV. **Results and Discussion.**

A. Gelation and Phase separation.

To search for the gel concentration, a total of 32 samples were prepared from the four ionic liquids. In the table 3 the physical state of each sample is reported. As explained in the previous chapter, after making the sample, it was exposed to an ultrasonic bath for two hours. This was done to ensure a homogeneous dispersion of the silica nanoparticles.

Table 3. Concentration and phase of the prepared samples.

[SMIM][TFSI]	
A200 Concentration	Phase Behavior
0.2wt%	Liquid
1.0wt%	Liquid
1.2wt%	Liquid
2.0wt%	Liquid
2.2wt%	Liquid
2.6wt%	Liquid
2.8wt%	Liquid
3.0wt%	Weak Gel
3.2wt%	Weak Gel
3.6wt%	Weak Gel
6.3wt%	Strong Gel

[C2MIM][TFSI]	
A200 Concentration	Phase Behavior
2.0wt%	Liquid
3.0wt%	Liquid
3.2wt%	Gel
3.8wt%	Gel
4.0wt%	Gel
6.4wt%	Strong Gel

[C5MIM][TFSI]	
A200 Concentration	Phase Behavior
2.0wt%	Liquid
3.0wt%	Liquid
3.3wt%	Liquid
3.5wt%	Weak Gel
3.8wt%	Weak Gel
4.0wt%	Weak Gel
6.1wt%	Strong Gel

[EtOHMIM][TFSI]	
A200 Concentration	Phase Behavior
0.2wt%	Liquid
2.5wt%	Liquid
3.2wt%	Liquid + Weak Gel
3.5wt%	Liquid + Weak Gel
3.7wt%	Liquid + Weak Gel
4.0wt%	Weak Gel
4.5wt%	Weak Gel
6 wt%	Strong Gel

The concentration of A200 in the samples is reported in weight percent (wt%) of silica to the total amount of the ionic liquid. The obtained values for the gelation concentrations are given in Table 4. The samples are characterized in liquid, weak gel or strong gel samples. The liquid samples flow inside the vial, the weak gels do not flow if turned upside-down, but if they are shaken they flow. One strong sample was found for every IL. These samples do not flow even when shaken manually.

Table 4. Gel concentrations, i.e. at this concentration the mixture starts behaving as a solid like material. [a]The [SMIM][TFSI] dispersion present a meniscus if turned upside down. [b][EtOHMIM][TFSI] presented phase separation in every concentration below 4 wt%, even though the 3.2 wt% shows gel and liquid phase at the same time.

Ionic Liquid	**Silica wt%**
[SMIM][TFSI]	3.0[a]
[C5MIM][TFSI]	3.5
[C2MIM][TFSI]	3.8
[EtOHMIM][TFSI]	4.0[b]

The values obtained for the gelation concentration are in agreement with literature for similar ionic liquids [13] [14]. Studies done in literature use silica concentrations high enough to gel the ILs, but they do not give much attention to an exact gel concentration. The values reported in table 4 are meant to be a precise gel concentration for A200. It is not yet clear what the mechanism for the gelation of the ionic liquids is. Watanabe and coworkers have tried to explain the physicochemical properties of protic and aprotic ionic liquids gels. However they have not discuss the basic mechanisms for the gelation of ionic liquids in detail. Figure 15 shows the ionic liquid gels for the concentrations mentioned in Table 4.

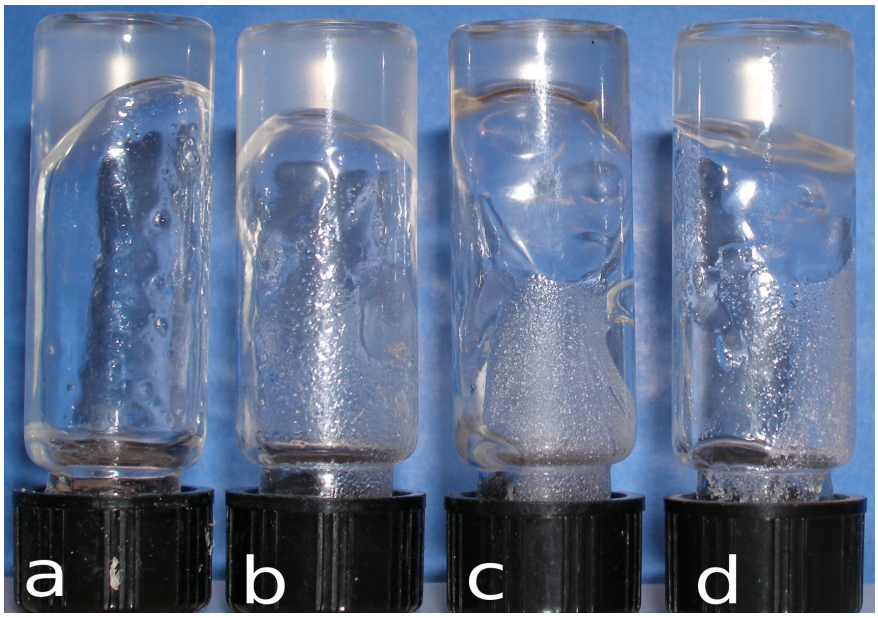

Figure 15. Ionic liquid gels of (a) [SMIM][TFSI], (b) [C5MIM][TFSI],(c) [C2MIM][TFSI], and (d)[EtOHMIM][TFSI]

Phase separation was observed for the ionic liquid dispersions with [EtOHMIM] [TFSI]. At low concentrations (~2 wt%) two types of fluid phases are present in the same sample, one of them more viscous than the other. At a 3.2 wt%, there was still phase separation, but for this concentration one phase was a gel and the other one was a viscous liquid (See Figure 16). If the silica concentration is increased even more, the amount of gel in the system increases as the amount of viscous liquid decreases, this behavior continues until 4.0 wt%. At this concentration, the sample is completely geled and there is no phase separation. For this ionic liquid, a strong gel was found at 6 wt% of particles. Phase separation does not occur for [C2MIM] [TFSI] even if the structure of the cation is similar. The reason for this phase separation is still unclear. The group of Watanabe [31] has reported phase separation of different ionic liquids in IL/poly(benzyl methacrylate) systems. Mixtures of [C1MIM][TFSI], [C2MIM][TFSI], [C4MIM][TFSI], and [C8MIM][TFSI] with poly(benzyl methacrylate) show a low critical solution temperature (LCST) phase behavior. From DSC experiments, they reported a negative entropy and enthalpy of mixing [31], which leads to phase separation of polymer and ionic liquids. The hypothesis of this research attributes the loss of mixing entropy to the formation of liquid clathrates, via associative interaction between the polymer and the ionic

liquid. To further investigate the phase separation of [EtOHMIM][TFSI] dispersions, further DSC experiments should be performed to determine the phase diagram. A reasonable hypothesis would take into account that the OH group on [EtOHMIM] changes the interaction of the IL with the A200 particles. The group of Watanabe reports [31] that a slight difference in the structure of the cation, such as the additional CH_3 in the alkyl chain in imidazolium based ILs, results in a big change (~20°C) in the critical temperature at which the mixture phase separates. In the case of this work, the addition of an OH group in the alkyl chain also changes the critical temperature.

The weak gel samples of show yield stress. This was checked by manually shaking the vial containing the sample (for [EtOHMIM][TFSI] this was checked at concentrations higher than 4 wt%). Before shaking the vial the samples do not flow flow, even if the vials are upside-down, but if the sample is shaken, the ionic liquid gel starts to flow. A short time (around one second) after the shaking stops, the sample acts as a solid-like material again. This experiment can be done several times without changing the outcome i.e. the sample changes from solid to liquid-like material if shaken and from liquid to solid-behavior when the shaking stops. When shaking the vials, it is possible that there is a disruption of the interparticle physical bonds, leading to a liquid-behavior on the material. Once the shaking stops, the bonds between nanoparticles are rapidly restored, this makes the material behave as a gel again. Even though all the weak gel samples presented this behavior, it is worth noting that the weak gels made of [SMIM][TFSI] are stiffer, i.e. to achieve yield stress a higher strength is needed. It is possible that [SMIM][TFSI] has a higher yield stress because the viscosity is the highest among all the ionic liquids.

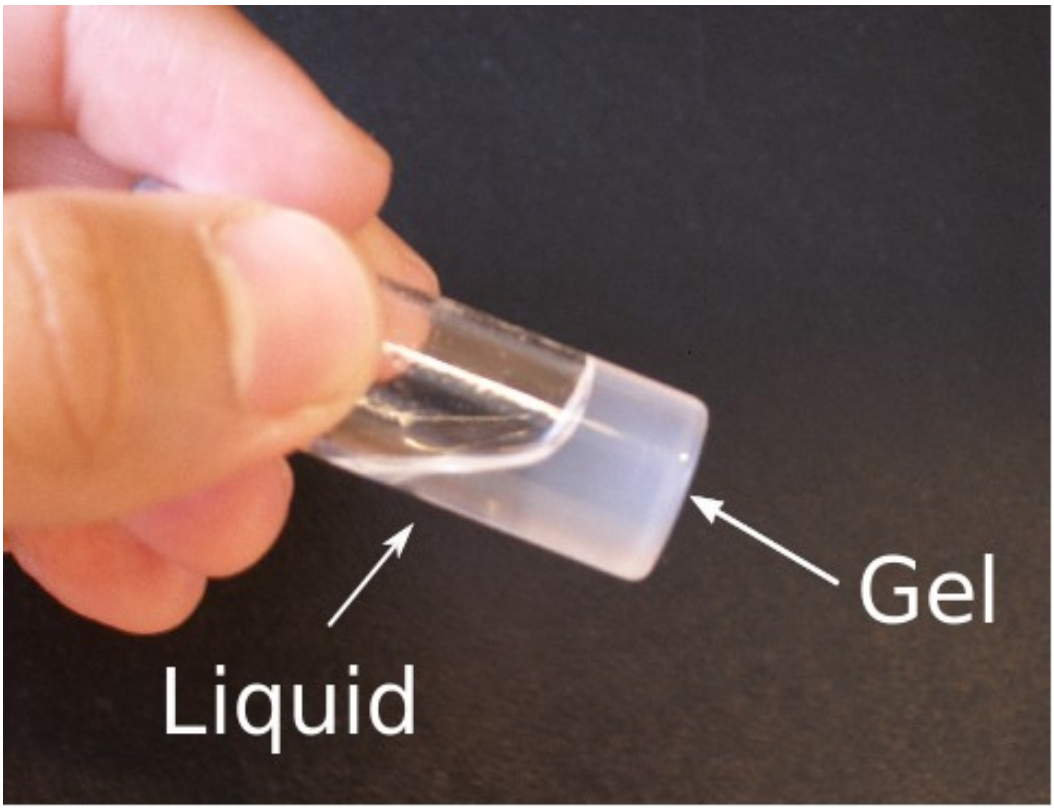

Figure 16. Phase separation in [EtOHMIM][TFSI] at 3.2 wt% A200 concentration.

Dispersions based on [SMIM][TFSI] presented an interesting phase behavior. Among the four ionic liquids, this one has the highest viscosity and glass transition temperature (-55°C). When mixing A200 nanoparticles and the ionic liquid, the fluid became more viscous until it formed a gel. At concentrations lower than 3wt%, the dispersion was a very viscous fluid. In the concentration range from 3 wt% to 3.6 wt % the colloidal dispersion shows an interesting behavior: when the vial was turned upside-down, the sample flows really slowly, but after flowing for a few seconds (30-90 seconds, depending of the silica concentration) the sample starts to act as a solid-like material. The behavior is reversible and the experiment can be repeated without any change in the behavior. At a concentration of 3.6 wt%, the sample is a weak gel: it does not flow when turned upside-down, unless shaking of the sample. These gels are sensitive to temperature variations, this was checked by heating the samples up to 50°C. When heated, the material flows faster, and the time at which the sample is flowing are reduced considerably (15-30 seconds). When [SMIM]

[TFSI] with 3.6 wt% of silica was heated at 50°C, there is no flow of the dispersion. Figure 17 shows a scheme of how the [SMIM][TFSI] gels with concentrations between 3 - 3.6 wt% behaves before and after turning the vial. It is worth noting that this behavior does not happen for [C5MIM][TFSI], even if the structures of the ionic liquids are similar.

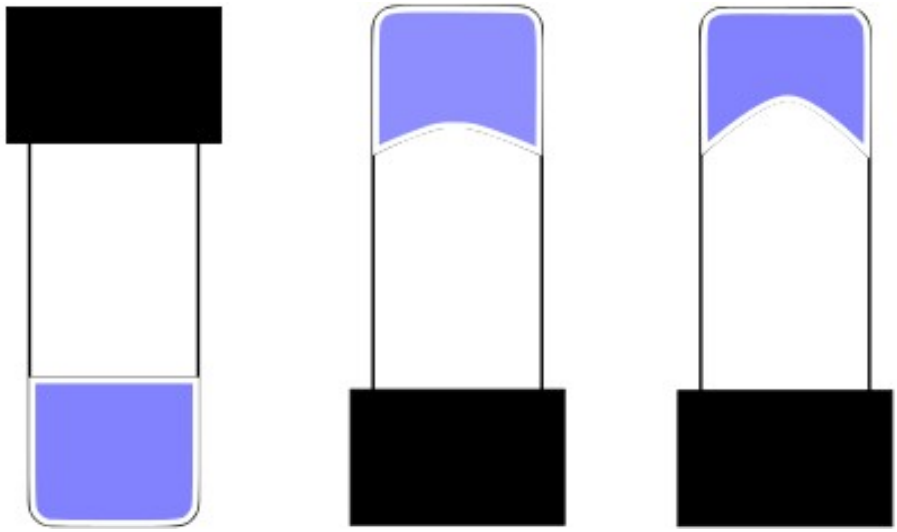

Figure 17. [SMIM][TFSI] gel behavior:(left) the weak gel is unperturbed, (center) when turned, the weak gel starts to flow, and (right) the gel reaches a final gel behavior.

To check the mechanical stability [32] of the ionic liquid gels, an experiment was done were a metallic sphere with a diameter of 4.5 mm and a weight of 372 mg was placed on top of the gel in the vial. This was performed for one sample of each type of IL: [C2MIM][TFSI] 3.8 wt%, [C5MIM][TFSI] 4w%, [SMIM][TFSI] 3.6%, and [EtOHMIM][TFSI] 3.2 wt%. The four samples (with the metallic sphere on the top) were then heated up to 110°C. At this temperature, none of the balls descend to the bottom of the sample. This indicates that up to 110°C, the gels are mechanically stable. It is worth noting that in the [SMIM][TFSI] 3.6% sample, bubbles started to appear around the metallic sphere at 110°C. To further check the stability of the gels a simple experiment was performed: once the metallic sphere was placed in the vial the gel were shaken. The result of this was that the spheres reached the bottom of the vial. After a few minutes, the samples are turned upside-down: the balls do not fall of the gel, unless there is some perturbation disrupting the structure of the gel (like

manually shaking the sample). In figure 18 a picture of the metallic ball inside the gel before and after turning, as it is clear, the gel is stable and the ball does not flow.

Figure 18. Metallic sphere experiment for [C2MIM] [TFSI] 3.8 wt% silica.

The metal ball experiment was also done for gels of [SMIM][TFSI] with concentrations 3 – 3.2 wt%. At room temperature, the ionic liquid gels with low silica concentration (3wt%) were not able to support the metallic sphere, i.e. the ball touched the bottom of the vial as soon as it was placed in the container. However, the sample with higher concentration (3.2 wt%) was able to support the ball at room temperature. When the gel sample (3.2 wt%) was heated at ~100°C, the ball goes to the bottom of the vial. This indicates that the interparticle interaction is not as strong as for the gel samples with higher silica concentration.

B. Glass Transition Temperature.

DSC measurements were performed to determine the glass transition temperature of the pure and gelled ionic liquids. By comparing different ionic liquids, it is noticed

that the differences in T_g can be related to two main factors: from the change in the length of the imidazolium side chain and from the addition of a side group in the alkyl chain. It is clear from Table 5, that the influence of the side group on the alkyl chain has stronger influence than the length of the alkyl chain, in agreement with literature [33] [34].

Table 5. Glass Transition Temperature of the pure ionic liquids.

Ionic Liquid	**Glass Transition Temperature**
[SMIM][TFSI]	-55°C
[C5MIM][TFSI]	-85°C
[EtOHMIM][TFSI]	-75°C
[C2MIM][TFSI]	-91°C

The variation of the glass transition temperature with A200 concentration is reported in Figure 19. Which clearly shows that T_g does not change significantly with the silica concentrations used in these experiments. The weak influence of the silica concentration on the glass transition suggests that on average there is not a very strong interaction between the ionic liquid and the silica nanoparticles, at least in this concentrations range.

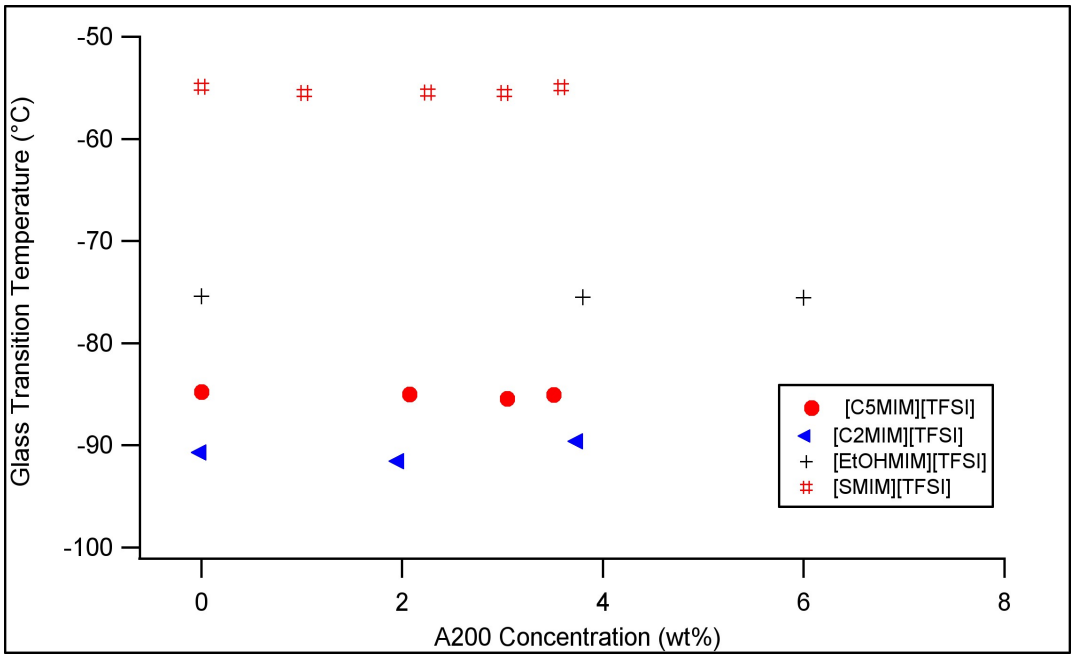

Figure 19. Glass transition temperature as a function of concentration of A200 nanoparticles. In none of the ionic liquids the T_g value changes considerably.

It is possible that the silica nanoparticles interact only with a small part of the ions in the ionic liquid. This would explain why the value for the T_g does not change importantly for increasing A200 concentration. However in literature it is reported [14] that when the concentration of silica nanoparticles is increased up to 15 wt%, the melting temperature decreases by 10°C. According to literature [14], the melting point decrease of the immobilized ionic liquids is caused by the interfacial effects and hydrogen bonding between the surface of silica and the ionic liquids.

C. Ionic Conductivity.

The aim of measuring the ionic conductivity in the ionic liquid gels and dispersions, is to understand the transport properties and the influence on the charge transport by silica concentration. Measurements were performed for dispersions with different A200 concentration. It would be natural to think that the conductivity would decrease as the material starts to behave as a solid, but surprisingly, the conductivity behaves similar in the ionic liquid gels and as in the pure ionic liquid.

Figures 20 and 21 show Arrhenius plots of the ionic conductivity for the ionic liquids and ionic liquid dispersions. In figure 20b and figure 21b, there is a scaling of the conductivity using the glass transition temperature. This is done to analyze how the conductivity depends on the glass transition temperature.

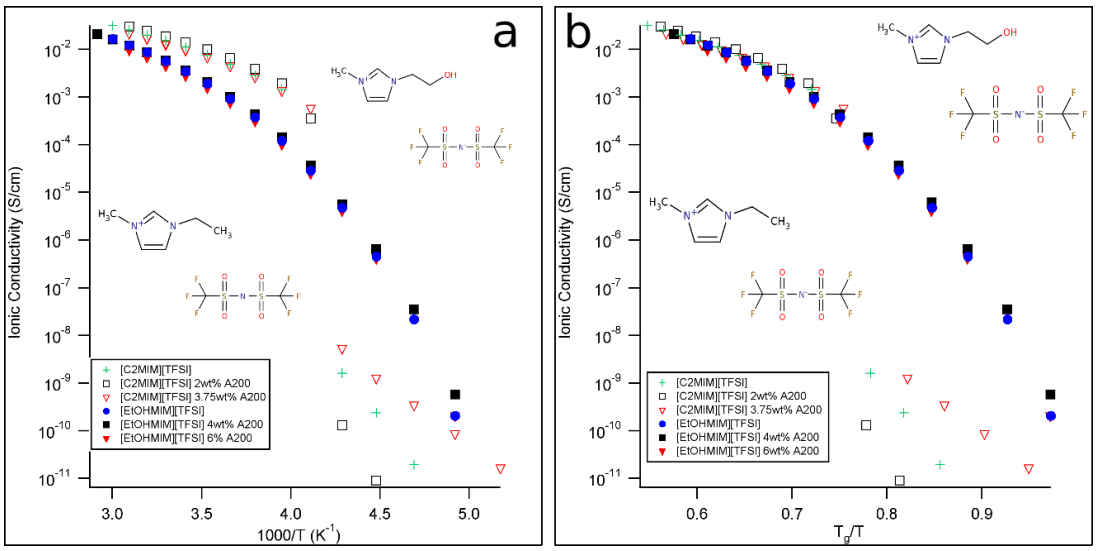

Figure 20. Conductivity as a function of inverse temperature for [C2MIM][TFSI] and [EtOHMIM][TFSI] for different A200 concentrations. In figure 19b a scaling of the temperature axis with glass transition temperature is used.

Figure 20a shows the ionic conductivity as a function of inverse temperature for [C2MIM][TFSI] and [EtOHMIM][TFSI] for different silica concentrations. As expected for ionic liquids, the conductivity follows a non-Arrhenius dependence [33]. For [C2MIM][TFSI], there is an abrupt change in the conductivity at ~-15°C, related to the crystallization of this ionic liquid (see the full DSC curve of [C2MIM][TFSI] in Figure 7). In the temperature range where the samples behave as liquids, the conductivity is slightly higher for a sample with silica particles rather than the pure ionic liquid. At 20°C, the sample with highest conductivity for [C2MIM][TFSI] dispersions is the one with 2.0 wt% silica (which is a liquid sample), the second highest conductivity is the pure ionic liquid, and the worst conductivity is found for the sample with a 3.5wt% concentration (which is a gel) (see figure 15). This suggest that the silica nanoparticles slightly enhance the conductivity of ionic liquid

dispersions at low silica concentration. However if the silica concentration is high enough, the silica lowers the conductivity of the dispersion.

For [EtOHMIM][TFSI] the conductivity behaves in a similar way since this ionic liquid phase separates for silica concentrations lower than 4wt%, the ionic conductivity was measured for gel (4 and 6wt%) and for the pure ionic liquid. No measurement of liquid dispersion was performed. Interestingly, a slightly higher conductivity is found for the sample with 4wt% silica, compared to the pure ionic liquid. The gel with 6wt% A200 has the lowest conductivity among the three samples. In literature [35] a higher conductivity it is reported for the pure ionic liquid compared to the gel samples for [C2MIM][TFSI], but the used concentrations in reference [35] are higher than the ones used in this work (5-15 w% silica).

Near room temperature (20°C) the conductivity of [EtOHMIM][TFSI] and [C2MIM][TFSI] are $2.16 \cdot 10^{-3}$ and $1.11 \cdot 10^{-2}$ S/cm respectively. At every temperature, [EtOHMIM][TFSI] presents a lower conductivity than [C2MIM] [TFSI]. This may be due to the fact that the [EtOHMIM] cation is heavier and bulkier than [C2MIM], thus reducing the diffusivity of the charge carrier. Also, the presence of an additional OH group on the cation might induce more hydrogen-bonds within the ionic liquid, leading to stronger ion-ion interaction, hence, reducing the mobility of charge carriers and decreasing the conductivity.

The scaling of the conductivity using the glass transition temperature for [EtOHMIM][TFSI], [C2MIM][TFSI] and the corresponding silica containing samples, are shown in Figure 20b. Even though there is not much change in the glass transition temperature with silica concentration, the conductivity values tend to align on the same curve for both ionic liquids. This indicates that both ionic liquids have the same temperature dependence of the conductivity. Furthermore, the results suggest that in [EtOHMIM][TFSI] and [C2MIM][TFSI] gel samples, the conductivity is closely related to the viscosity of the pure ionic liquids, rather than the viscosity of the ionic liquid gels.

In Figure 21 the temperature dependence of conductivity is shown for [C5MIM][TFSI] and [SMIM][TFSI]. Similar to the other two ionic liquid dispersions, the conductivity is higher for the samples containing [C5MIM][TFSI], since the cation is smaller and lighter than the [SMIM] cation. The conductivities at room temperature (~20°C) of [C5MIM][TFSI] and [SMIM][TFSI] are $3.4 \cdot 10^{-3}$ and $2.5 \cdot 10^{-4}$ S/cm. For both dispersions, the conductivity dependance on concentration is similar. The conductivity of the liquid material is the slightly higher than for the gel material. For [C5MIM][TFSI] at room temperature, the conductivity is higher for the pure ionic liquid than for the ionic liquid gel (3.8 wt%). In a similar way, for [SMIM][TFSI], the sample with higher conductivity is the one with 2.2 wt% silica (which is a viscous liquid at room temperature), the second highest conductivity is found in the pure ionic liquid, and finally, the sample containing 3.6 wt% of A200 (which acts as a solid material at room temperature)

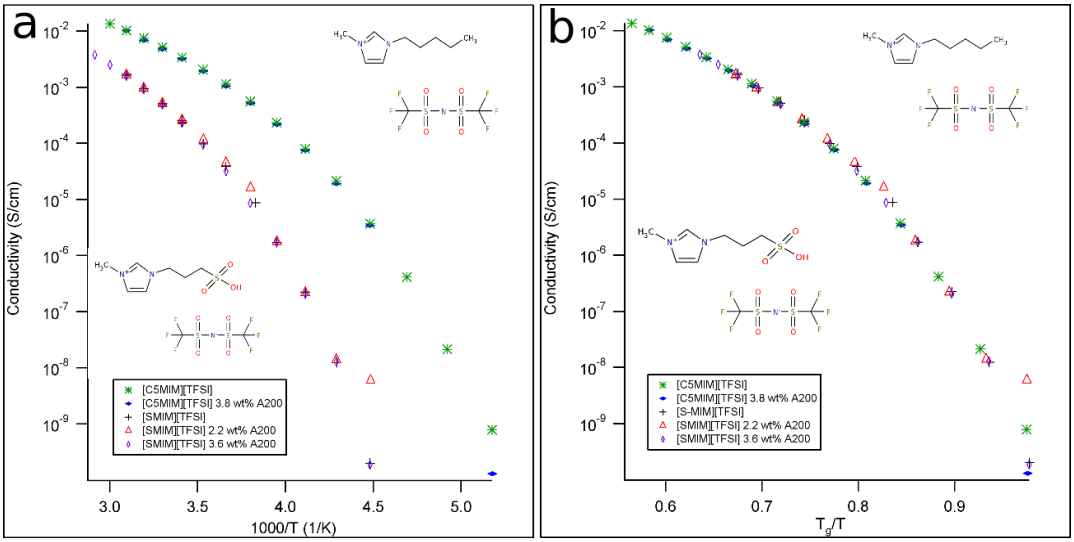

Figure 21. Conductivity for [C5MIM][TFSI] and [SMIM][TFSI] as a function of temperature. (a) shows the arrhenius plot, (b) presents the scaling with the glass transition temperature.

Conductivity scaling with T_g in Figure 21b, shows that the conductivities of the two ionic liquids present the same temperature dependence. This shows that the conduction process is dominated by the viscous properties of the ionic liquid component, rather than the viscosity of the ionic liquid gels.

It is reported in literature that the addition of silica nanoparticles slightly decreases the ionic conductivity due to a decrease in anion and cation mobility [35]. Nevertheless, in this work it is found that when the dispersions have a low silica concentration, the ionic conductivity is slightly enhanced. Even though it is not clear why this happens, a possible explanation would consider that when adding silica to the IL, some impurity from the A200 nanoparticles could be introduced in the dispersions. If the material has a low silica concentration, these impurities could enhance the ionic conductivity. If the silica concentration is high enough, the contribution of the impurity could be decreased due to the space restrictions imposed by the silica particles. Possible impurities of A200 nanoparticle are listed in reference [25]

D. Molecular Interactions

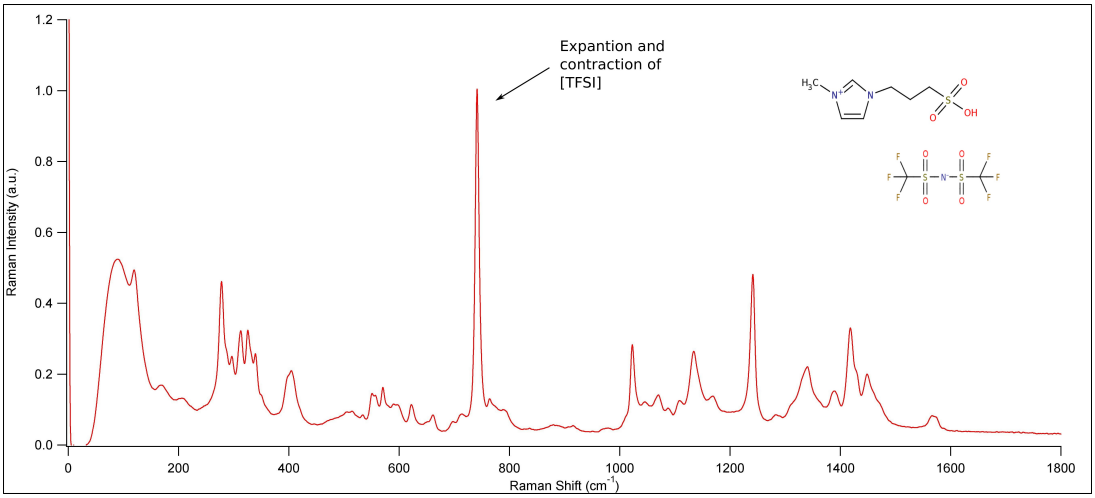

Figure 22. Raman spectrum for [SMIM][TFSI].

In the Raman spectra of the ionic liquid gels there are many bands to search for vibrational information. In figure 22 the Raman spectrum for [SMIM][TFSI] is shown. Nevertheless, in this thesis the interest is focused on the 740 cm^{-1} band, which corresponds to the expansion and contraction of the hole TFSI anion [30]. The [TFSI] anion can exist in two conformations, a transoid (C_1) and a cisoid form

(C_2). In the C_1 symmetry, the CF_3 groups are both at the same side of the S-N-S plane while in the C_2 symmetry the CF_3 groups are in opposite sides of the plane, see Figure 23. The two conformations are able to co-exist in the ionic liquid, and the conversion between them requires only a few kJ/mol, hence, TFSI is very flexible. Ab-initio calculations have shown that the Raman shift difference between the two conformations is around 3 cm^{-1} [36] and that the corresponding Raman cross-sections are nearly equal. Hence the spectral component of the anion at 740cm^{-1} is the sum of the contributions of the C_1 and C_2 conformations. In addition to conformational effects, the band is very sensitive to interactions [36].

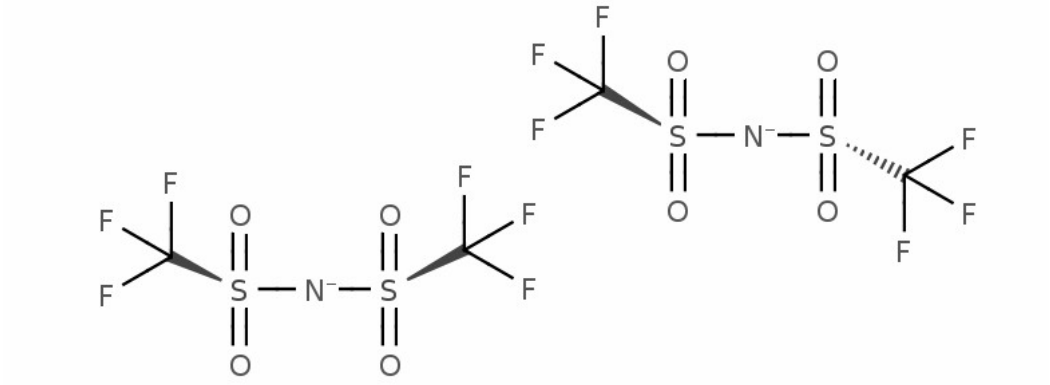

Figure 23. Two conformations of [TFSI] anion transoid (left) and cisoid (right) symmetry

The 740 cm^{-1} vibrational mode for TFSI in the pure ionic liquids is shown in Figure 24. It is possible to see that there are shifts in the 740 cm^{-1} peak for the ionic liquids. The differences in the vibrational modes are most likely related to changes in the conformation of the TFSI, from the change in the C_1/C_2 ratio. The peaks are located approximately at 740.5 cm^{-1} for [C2MIM][TFSI], 741.1 cm^{-1} for [EtOHMIM][TFSI], 740.4 cm^{-1} for [C5MIM][TFSI], and 741.3 for [SMIM][TFSI]. From the shift in these peaks, it is possible to conclude that there is a higher change from the influence of the addition of a side group in the alkyl chain than the length of the side chain of the imidazolium ring.

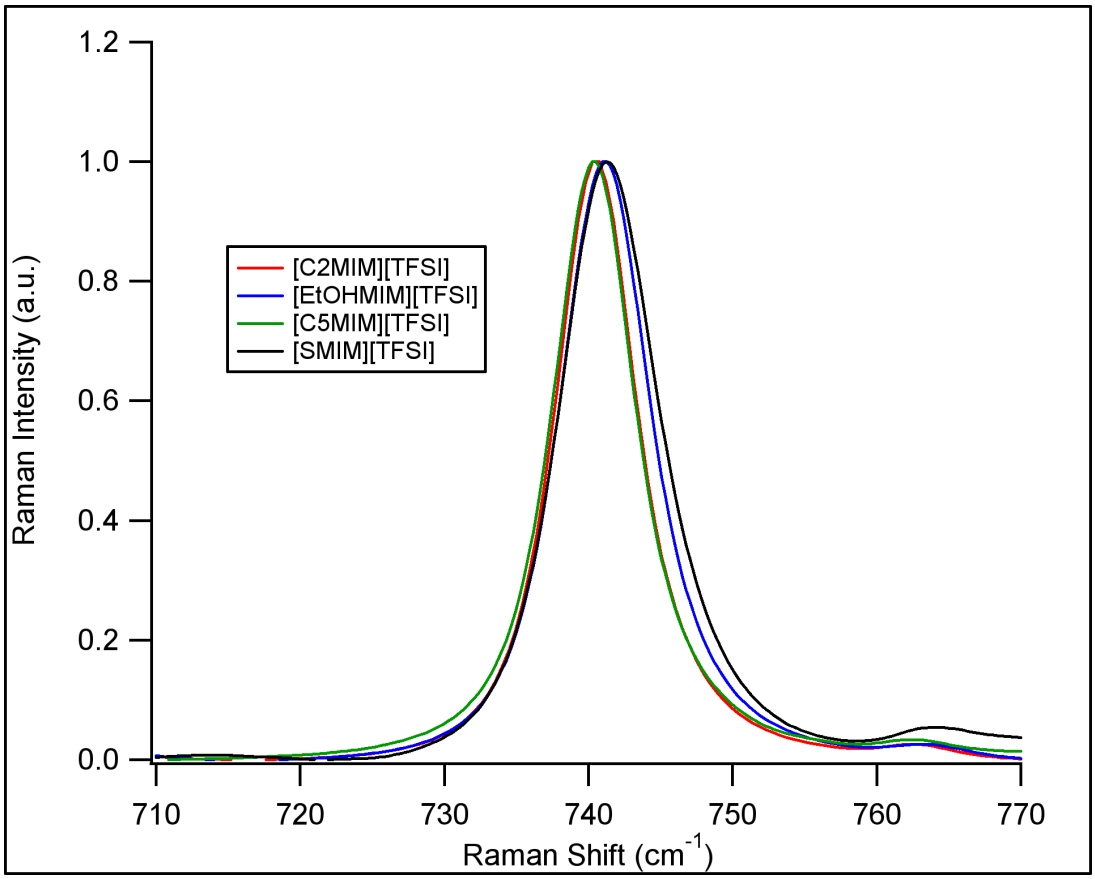

Figure 24. Raman Spectra of 740 cm⁻¹ vibrational mode for the pure ionic liquids.

Figure 25 shows the 740 cm $^{-1}$ band for all ionic liquid gels. All spectra were normalized to the peak maximum. The background was subtracted from every spectra in order to compare the results for different silica concentrations. Once background is subtracted and the band is normalized, the peaks from each ionic liquid overlap perfectly from 710 to 770 cm⁻¹. This indicates that there is no change of the vibrational mode of [TFSI] as the silica concentration increases, suggesting that there is no change in conformation or ionic interactions of the [TFSI] anion as the amount of silica increases.

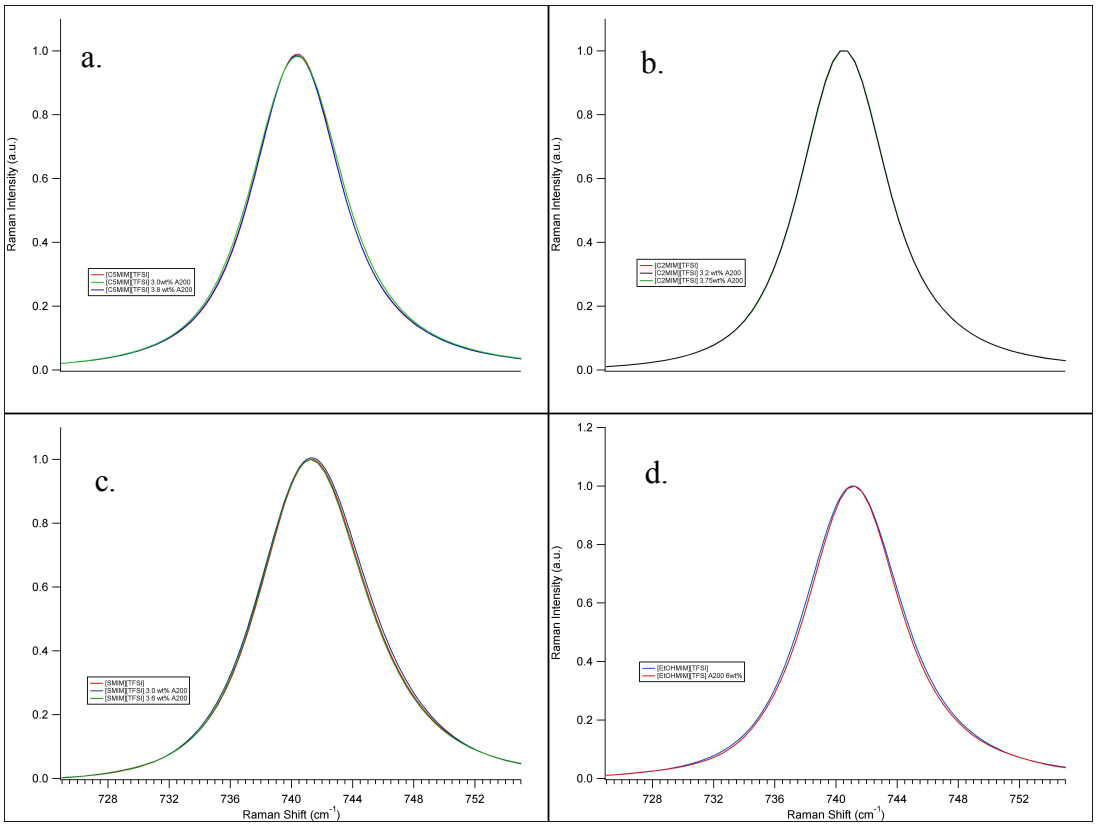

Figure 25. Raman Spectra for 740 cm⁻¹ band for (a) [C5MIM][TFSI], (b) [C2MIM][TFSI], (c) [SMIM][TFSI] and (d) [EtOHMIM][TFSI]

V. Conclusions and Further Work

Using A200 silica nanoparticles as a dispersed media, the ionic liquids: [SMIM][TFSI], [C5MIM][TFSI], [C2MIM][TFSI], and [EtOHMIM][TFSI] made stable gels. For each ionic liquid gel, a different gel concentration was found. The phase of the dispersions were characterized as liquid, gel, and strong gel. Results from differential scanning calorimetry and dielectric spectroscopy, suggest that there is no considerable influence of the A200 nanoparticles on the glass transition temperature or ionic conductivity of the dispersion or gels, up to the reached silica concentration. Using Raman spectroscopy, it was determined that there is not an important influence of A200 on ionic interactions/conformation of TFSI, this was determined up to the concentrations used in this work. A possible explanation is that the matrix of silica nanoparticles act as a "container" for the ionic liquids: even though the A200 nanoparticles are able to arrest the ionic liquid, they do not change significantly thermal, ionic conductivity or vibrational properties of an ionic liquid. Results suggest that the physical properties of pure ionic liquids are determined by the structural differences of the ions, in this case, the length and end group of the alkyl side chain on the cation. Usually, the end group of the side chain of the imidazolium cation is of greater importance than the length of the chain.

Phase behavior was studied using a metallic sphere method. It was proven that the ionic liquids form stable gels with A200 nanoparticles from room temperature until 110°C. The ionic liquid gel [EtOHMIM][TFSI] phase separates at concentrations lower than 4wt% A200.

In the line of work of this thesis, some research ideas that could improve this work are:

- Measure the temperature dependence of viscosity of the ionic liquid gels.
- Perform Photon Correlation Spectroscopy on the samples, this to obtain the hydrodynamical size of the particles and the variation with A200

concentration.

- Perform rheological measurements for the gels, measuring elastic and viscous moduli to characterize mechanical properties of gels, weak gels and liquid dispersions.
- Perform infrared Spectroscopy to study hydrogen bonding between silica nanoparticles.

Bibliography

1. Wang, P.; Zakeeruddin, S. M.; Exnar, I.; Grätzel, M.; Journal of the American Chemical Society. 125, 1166-1167 (203)

2. Stathatos, E.; Lianos, P.; Zakeeruddin, S. M.; Grätzel, M.; Chemistry of Materials. 15, 1825-1829 (2003)

3. Seki, S. et al., J. Phys. Chem B. 110, 10228–10230 (2006)

4. Matsumoto, H., et all, J. Power Sources. 160, 1308-1313 (2006)

5. Gorlov, M.; Kloo, L.; Dalton Trans. 20, 2655-2666 (2008)

6. M. Freemantle, Introduction to Ionic Liquids. RSC Publishing, (2010)

7. Armand, M.; Endres, F.; MacFarlane, D. R.; Nat. Mat. 8, 621-629 (2009)

8. Welton T., Chem. Rev. 2071 (1999)

9. Wasserscheid, P; Keim, W; Angew Chem. Int. Ed. 39, 3772 (2000)

10. R.A.L Jones, Soft Condensed Matter Physics, (2002).

11. Klaas te Nijenhuis; Thermoreversible Networks, (1997).

12. Heremans, PH.; Colloidal Science II, (1949).

13. Ueno, K.; Imaizumi, S.; Hata, K.; Watanabe, M.; Langmuir. 25, 825-831 (2009)

14. Liu, Y.; Wu, G.; Fu, H.; Jiang, Z.; Sha, M.; Dalton Transactions. 39, 3190-3194 (2010)

15. Ueno, K.; Inaba, A.; Kondoh, M.; Watanabe, M.; Langmuir. 24, 5253-5259 (2008)

16. Ueno, K.; Inaba, A.; Ueki, T.; Watanabe, M.; American Chemical Society. 26, 18031-18038 (2010)

17. Ueno, K.; Inaba, A.; Kondoh, M.; Watanabe, M.; Journal of Physical Chemistry. 114, 13095-13103 (2010)

18. Jonas Nordtröm, Structure and Dynamics of Silica Dispersion and Gels, 2009.

19. IUPAC Compendium of Chemical Terminology, 66, (1997)

20. Trofymluk, O.; Levchenko, A.; Navrotsky, A; Journal of Chemical Physics. 123, 194509-1 - 194509-7 (2005)

21. Sergei V, Dzyuba, Chem. Phys. Chem. 3, 161-166 (2002)

22. Fredlake C. P.; Crosthwaite J. M.; Hert D. G.; J. Chem. Eng. Data. 49, 954 - 964 (2004)

23. Dzyuba S. V., Bartsch R.; Tetrahedron Letters. 43, 4657-4659 (2002)

24. Bonhote P.; Dias A. P.; Papageorgiou N; Inorg. Chem. 35, 1168-1178 (1996)

25. Technical Bulletin Fine Particles, 11, (1967)

26. P. J. Haines, Thermal Analysis and Calorimetry, (2002).

27. Jagath Pitawala, Structure-Property Relationship of Ionic Liquids and Their Li Salt Mixture, 2010.

28. Kremer, F.; Schonhals, A; Broadband Dielectric Spectroscopy, (2003).

29. Smith, Ewen; Dent, Geoffrey, Modern Raman Spectroscopy -A Practical Approach, (2005).

30. Martinelli, A.; Matic, A.; Johansson P.; Jacobsson P.; Bjorsson, L.; Journal of Raman Spectroscopy. 42, 522-528 (2010)

31. Ueki, T.; Kodama, K.; Kaino, S.; Takeshi, M.; Watanabe, M.; Pure Appl. Chem. 81-10, 1829–1841 (2009)

32. Yoshito, O.; Kanji, K.; Gels Handbook, (2001).

33. MacFarlane, D. R.; Pringle, J. M.; Johansson, K. M.; Forsyth, M.; Chem Communications. 1905, (2006)

34. Greaves, T. L.; Weerawerdena, A.; Fong, C.; Drummond, C.; J. Phys. Chem B. 110, 22479-22487 (2006)

35. Ueno, K.; Kenji, H.; Toru, K.; Masashi, K.; Watanabe, M.; J. Phys. Chem. B. 112, 9013-9019 (2008)

36. Rey, I.; Lassègues, J.C.; Grondin, J.; Servant, L., Electrochimica Acta. 43, 1505-1510 (1998)